Journal of Chemical&Engineering Data

pubs.acs.org/jced

Article

Gas Solubility Modeling of Ethylene in Semicrystalline Polyethylenes with Different Macromolecular Architectures Based on a Thermomechanics Approach

Jana Zimmermann, Sabine Enders, and Michael Fischlschweiger*

Cite This: https://doi.org/10.1021/acs.jced.3c00429

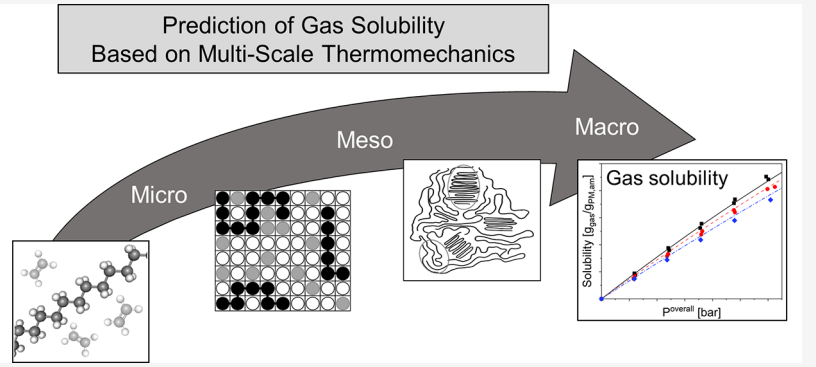

ABSTRACT: The solubility of gases in semicrystalline polymers is a significant property with numerous applications, such as gas-phase polymerization. Although thermodynamic modeling has successfully determined gas solubility in glassy polymers or polymer melts without crystallites, predicting gas solubility in polymers with a semicrystalline morphology remains challenging. This study presents a novel multiscale modeling approach based on thermomechanics to predict gas solubility in semicrystalline polymers across different temperatures, pressures, and various grades of polyethylene. The thermomechanical framework incorporates the SL-EOS and continuum mechanics, utilizing a mechanical homogenization method to consider the semicrystalline morphology and obtain local mechanical material information. Additionally, the temperature dependence of the degree of crystallinity of polyethylene is considered. By employing this approach, the solubility of ethylene in different polyethylene grades in the semicrystalline state can be accurately predicted, demonstrating good agreement with experimental data with a relative error below 3%.

1. INTRODUCTION

The investigation of gas solubility behavior is a significant topic in several application fields like biological drug engineering, chemical engineering, and material science.[1−5]

Especially the thermodynamic modeling of gas solubility in polymers plays an essential role in many different applications such as gas phase polymerization, development of gas separation membranes, recycling by supercritical extraction for purification of contaminated polymers, production of foam materials for insulation and packaging, or optimization of fuel cells with durable membranes.[6−10]

The phenomenon of gas solubility in a semicrystalline polymer is complex, and influenced by a broad spectrum of variables. These include ambient conditions such as pressure and temperature. However, the gas sorption ability of a polymer relies on various factors including solvent structure, as well as the polymer type and the specific macromolecular architecture of the polymer, e.g.. chemical composition, molecular weight distribution, branching, and further the semicrystalline morphology, e.g., degree of crystallinity and crystal geometries. The molecular architecture affects the overall solubility process due to the unique entanglement of polymer molecules influenced by the molecule length and their branching. In semicrystalline polymers, the morphology is built of coexisting crystalline and amorphous domains varying significantly in their ability to dissolve gas. It is known that gas solubility predominantly occurs in the amorphous phase, leading to a state of heterogeneous solubility.[11,12] Consequently, this results in a heterogeneous intrinsic pressure distribution within the semicrystalline polymer.[13] The crystalline regions, with folded chains and ordered lamella,

Special Issue: In Honor of Gabriele Sadowski

Received: July 10, 2023
Accepted: September 22, 2023

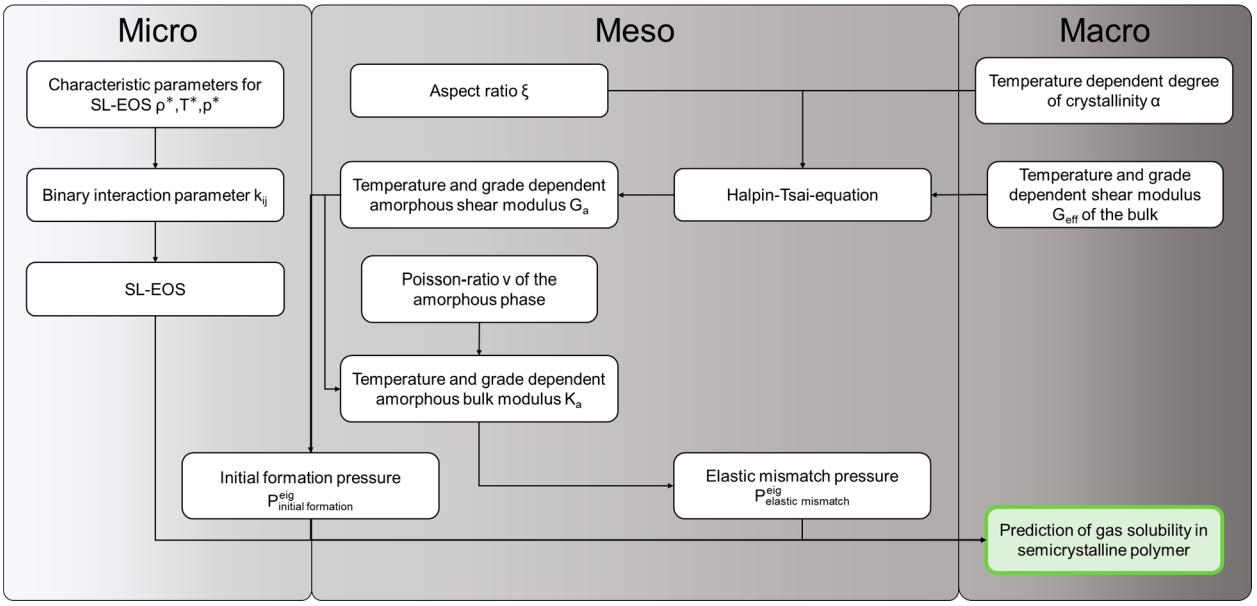

Figure 1. Schematic description of the multiscale modeling approach to predict the gas solubility in a semicrystalline polymers.

present barriers to gas solubility. They tend to influence the unrestrained expansion of the amorphous phase induced by gas sorption. This inherent restriction by crystalline domains results in a unique interplay of eigenstresses within semicrystalline polymers, triggering gas solubility behavior intricately. Due to the difficulty in providing a comprehensive description of the morphological and mechanical perturbation felt by the amorphous phase and the interaction with the crystalline regions, it is still a challenging task to predict the gas solubility in semicrystalline polymers.

Generally, one viable approach to model the solubility of gas is the Perturbed-Chain Statistical Associating Fluid Theory-EOS (PC-SAFT) developed by Groß and Sadowski.[14,15] Many works utilized this EOS to describe the gas solubility behavior successfully. For instance, Wiesmet et al.[16] modeled the high pressure-phase-equilibria of polyethylene glycol with various inert gases.

Vogelpohl et al.[17,18] investigated the gas solubility in multicomponent systems with PC-SAFT[14,15] and accomplished the prediction of the CO solubility in organic compounds. Tumakaka et al.[19] modeled various complex systems, containing associating and polar as well as nonpolar substances with PC-SAFT.[14,15] In the work of van Schilt et al.,[20] PC-SAFT[14,15] was used to predict the high-pressure phase behavior of poly(cyclohexene carbonate) and cyclohexane oxide and CO_2, where a good agreement between experimental and modeling results could be shown. Schäfer et al.[21] combined the density gradient theory with PCP-SAFT[22] to model the interfacial properties in various vapor−liquid- and liquid−liquid-equilibria. Hassanpouryouzband et al.[3] showed the prediction capability of PC-SAFT by investigating the solubility of heavy components in hydrocarbons.

As in previous works[23−26] already demonstrated, the Sanchez−Lacombe EOS (SL-EOS)[27,28] is, besides PC-SAFT,[14,15] one suitable EOS to describe gas solubility in molten polymers. Several groups[11,29,30] however showed in their work, that the solubility of gas in polymers changes significantly below the melting temperature of a semicrystalline polymer. The reason for this is that in principle solvent can only penetrate the amorphous phase and the solubility in crystals is very small and hence negligible[12] or even nonexistent.[11] In addition to the mesophase character, it can be found that the amorphous phase shows itself a reduced ability to uptake gas in the semicrystalline polymer state.[11] The reason is that the amorphous phase is hindered by the crystallites present which act as a kind of constraint.[11−13] Amorphous molecules with their ends directly linked to the crystalline lamella, also referred to as tie molecules, seem to affect the overall amorphous matrix[11,31] resulting in a different density state of the amorphous phase (compared to a nonrestricted state at equal temperature and pressure)[30] as well as a reduced mobility of the macromolecules. Different groups incorporated these findings into thermodynamic modeling. For example, Bonavoglia et al.[30] used a Non-equilibrium Lattice Fluid Model (NELF) and Memari et al.[32−34] and Minelli and De Angelis[12] embedded an additional constraint pressure as an adjustable parameter. Michaels and Haussleix,[35] Sturm et al.,[11] and Valsecci et al.[31] included an elastic force, which the tie chains exert onto the amorphous phase like a spring,[36−38] by integrating an energy contribution into the modeling as an adjustable parameter. These parameters cannot be experimentally determined or predicted based on the pure substances, rather they are determined based on corresponding solubility data of the mixture, where the polymer is in the semicrystalline state. Following these procedures the mentioned approaches[24,26,31−34,39−43] lead to good agreement between thermodynamic modeling results and measured solubility data. An additional approach was recently developed by Fischlschweiger et al.,[13] where the goal was to predict gas solubility in polymers, without using solubility information in the semicrystalline state, but rather considering the mechanics behavior of the pure polymer. To achieve this, the eigen pressure P^{eig} in the amorphous phase was calculated by coupling the SL-EOS with a mechanics approach. Based on this framework the induced eigen pressure by dissolving *n*-butane and *i*-butane in low-density polyethylene at low degrees of crystallinity was calculated, and the gas solubility could be predicted in the semicrystalline state for low-temperature isotherms.[13]

https://doi.org/10.1021/acs.jced.3c00429
J. Chem. Eng. Data XXXX, XXX, XXX−XXX

In this work, we will set up on ref 13 and further develop this method with a new multiscale approach that incorporates the geometric shape of crystals and the temperature-dependent mechanical properties of the amorphous phase of the pure polymer. Based on this the gas solubility in semicrystalline polymers showing higher and more complex semicrystalline morphologies should be predicted. To get access to the mechanical characteristics of the amorphous domains and for considering the crystals' domain geometry, a continuum mechanical homogenization method will be applied. With the new framework various semicrystalline polyethylene−ethylene systems, particularly those with higher levels of crystallinity, will be investigated. To ensure accuracy and reliability, this approach will be validated using experimental data from the literature. Furthermore, the temperature- and system pressure-dependent development of the amorphous and crystalline eigen pressure of these higher crystalline materials is calculated and discussed to get deeper insights into the morphology-dependent eigen pressure evolution in semicrystalline polyethylenes which show a different macromolecular architecture.

The structure of this paper is as follows: First, the applied methods will be outlined and explained, providing a comprehensive explanation of the thermomechanic framework and the required material parameters for prediction. Subsequently, a multiscale approach will be applied to predict the gas solubility of ethylene in different polyethylene grades. Finally, these predictions will be validated by comparing them with data from existing literature. Additionally, a further investigation will be conducted to analyze the distribution of eigen pressure within both amorphous and crystalline domains.

2. METHODS

In this section, the developed thermomechanic framework and the therefore needed material parameters as well as the interaction parameter for the mixtures will be systematically presented. To enhance clearness, in Figure 1 an overview of the multiscale modeling approach is presented. This representation outlines the key aspects and tasks involved in this study and shows how the scales and the information between the scales are connected.

To predict the gas solubility in a semicrystalline polymer, a connection between the macro-scale-property gas solubility and microscale thermodynamic modeling via an equation of state needs to be established. In this work on the microscale, the SL-EOS with consideration of an eigen pressure from Fischlschweiger et al.[13] will be used to model the gas solubility in semicrystalline polyethylene. This study expands upon the framework of ref 13 by incorporating a homogenization method to integrate the crystal geometry and the mechanical temperature-dependent moduli of the amorphous phase at the mesoscale. Additionally, this work accounts for the temperature-dependent degree of crystallinity when calculating gas solubility on the macroscale, which was not previously addressed in ref 13 but is introduced here in this paper.

For the EOS, the characteristic parameters of the pure components as well as the binary interaction parameter are necessary. The characteristic parameters of the pure polymer will be determined in this work by modeling *P-v-T* data from various polymer grades. Moreover, modeling the binary solubility data of the gas-polymer melt gives access to the binary interaction parameter of the mixture. The eigen pressure P^{eig} consists of two parts, the initial formation pressure $P^{eig}_{initial\ formation}$ and the elastic mismatch pressure $P^{eig}_{elastic\ mismatch}$. The initial formation pressure accounts for fracture mechanical forces, which are dependent on the temperature-dependent shear modulus of the amorphous phase. The elastic mismatch pressure is dependent on the restricted expansion of the semicrystalline polymer and therefore on the temperature-dependent compressive modulus of the amorphous phase, which will be determined by the shear modulus and the Poisson ratio of the amorphous phase. In this contribution, a mesoscale bridging via the Halpin−Tsai equation as homogenization method will be applied.

In the following section, the thermodynamic framework and the coupling of micromechanics into this approach will be explained.

2.1. Thermodynamic Framework. To predict the gas solubility in semicrystalline polymers, a further development of the thermodynamic framework based on the SL-EOS with eigen pressure from Fischlschweiger et al.[13] will be used. Herein, we provide the modeling framework and newly formulated equations, while expressions for equations, which are already published and used in this work from ref 13 are not presented again, rather readers are referred to ref 13 to get further details.

According to the assumptions above, the gas can only solve into the amorphous parts of the semicrystalline polymer, so that the chemical potential of the solute in the polymer phase μ_1^P is equal to the chemical potential of the solute in the amorphous phase $\mu_1^{P,am}$ and reads[13]

$$\mu_1^{P}(T, P^{overall}, w_1^{P}) = \mu_1^{P,am}(T, P^{am}, w_1^{P,am}) \quad (1)$$

with $w_1^{P,am}$ as the weight fraction of the gas in the amorphous phase and P^{am} as the pressure in the amorphous phase. Under mechanical equilibrium, the overall system pressure $P^{overall}$ equals the pressure of the gas phase P^G, so that eq 1 can be denoted as[12,13]

$$\mu_1^{G}(T, P^{overall} = P^{G}) = \mu_1^{P,am}(T, P^{am}, w_1^{P,am}) \quad (II)$$

To determine the weight fraction of the solute in the polymer phase w_1^P, the weight fraction of the solute in the amorphous phase can be converted with the degree of crystallinity α, so that $w_1^P = (1 - \alpha)\cdot w_1^{P,am}$.

It could be shown in ref 13 that the pressure of the amorphous phase P^{am} is the sum of the overall pressure of the system conditions $P^{overall}$ and the eigen pressure P^{eig} multiplied by the degree of crystallinity α (eq III).

$$P^{am} = P^{overall} + \alpha\cdot P^{eig} \quad (III)$$

As mentioned above, the eigen pressure P^{eig} consists of two terms, on the one hand the initial formation pressure $P^{eig}_{initial\ formation}$ and on the other hand the elastic mismatch pressure $P^{eig}_{elastic\ mismatch}$. As the first gas bubbles solve into the amorphous polymer, they form randomly distributed islands of penetrant molecules which lead to a microscopic expansion of the molecular entanglement at very low solute concentrations. This phenomenon is in accordance with the initial stretching of the tie chains between the crystalline lamellas when the solvent is penetrating the system and represents the first term of the eigen pressure, the initial formation pressure. In a simplified form under the assumption of highly reduced microscopic areas of the initial penetrant islands, the initial formation pressure can be described by equation (IV)[13]

https://doi.org/10.1021/acs.jced.3c00429
J. Chem. Eng. Data XXXX, XXX, XXX−XXX

$$P^{\text{eig}}_{\text{initial formation}} = 2.5G_a(T, \alpha, \xi) \quad \text{(IV)}$$

where G_a represents now the shear modulus of the amorphous phase at a certain temperature T, degree of crystallinity α, and aspect ratio ξ of the crystals, in this work the ratio of the crystal length to radius.

The second term, the elastic mismatch pressure, accounts for the interaction of the crystalline phase with the amorphous phase by inhibiting the volume expansion of the amorphous polymer. Due to the solute entering the amorphous matrix, the matrix swells which results in an isotropic and elastic mismatch between the crystalline and amorphous phases. This phenomenon can be described by[13]

$$P^{\text{eig}}_{\text{elastic mismatch}} = K_a(T, \alpha, \xi)\left(\frac{\Delta\tilde{V}}{\tilde{V}}\right) \quad \text{(V)}$$

where now $K_a(T,\alpha,\xi)$ is the bulk modulus of the amorphous phase at a certain temperature T, degree of crystallinity α. and aspect ratio ξ of the crystals. The term $\left(\frac{\Delta\tilde{V}}{\tilde{V}}\right)$ accounts for the relative volume change of the amorphous phase induced by solvent penetration. It is important to note that the reference state $\tilde{V}$ corresponds to the reduced volume of the pure amorphous polymer under the same state conditions (temperature and pressure P^{am}) as the amorphous phase of the semicrystalline polymer.

The theory, as stated in Fischlschweiger et al.[13] and applied in this work, considers uniform pressure fields, where crystallite geometry is not considered.

To predict the eigen pressure and thereby the solubility of gas in the semicrystalline polymer, several material parameters need to be determined through experimental methods of the pure polymer. In the following sections, we will provide an overview of the approach to determine the polymer parameters from various experiments.

2.2. Temperature Dependent Degree of Crystallinity. The pressure in the amorphous phase is directly affected by the crystalline domains and therefore the degree of crystallinity through the eigen pressure contribution. This can be observed in semicrystalline polymers, where the presence of crystalline regions restricts the solubility of gas, leading to lower solubilities at higher degrees of crystallinity.[42] With increasing temperature, the degree of crystallinity decreases until the polymer reaches a fully amorphous state once it surpasses its melting temperature. Consequently, while fewer crystals are present, the decrease in constraint pressure leads to enhanced gas sorption. However, at elevated temperatures, gas sorption is hindered due to the increased kinetic energy of the gas molecules resulting in greater intermolecular forces, which need to be overcome. These conflicting effects make it challenging to predict the gas solubility in semicrystalline polymers accurately. Therefore, it is crucial to determine the degree of crystallinity at each sample temperature; otherwise, there may be an underestimation of solubility levels.

The temperature-dependent degree of crystallinity has been studied in previous works.[44,45] By using mathematical correlations of experimental results, it is possible to determine both the degree of crystallinity at each sample temperature and the melting point of the polymer. The correlations are presented in the results section.

2.3. Shear Modulus of the Amorphous Phase: Halpin−Tsai Equation. Experimental data on the temperature- and crystallinity-dependent effective shear modulus of the bulk can be found in previous literature.[46] However, these data only refer to the property of the bulk and do not describe the amorphous phase, which is considered in the determination of the eigen pressure. Therefore, a mechanical homogenization method is one solution to get access to the shear modulus of the amorphous phase. The Halpin−Tsai equation[47,48] can serve as a simple method for this purpose. This equation is most often used to describe properties of a composite matrix reinforced with short inclusions with lower bound as the series model and upper bound as the parallel model. In this case, the composite matrix is represented by the amorphous phase and the inclusions with the crystal phase of the polymer. In general, predictions with the Halpin−Tsai model show accurate results for moderate inclusion volume fractions, which is appropriate for the investigated polymer grades in this work.[49,50] Deviations become more prevalent at greater inclusion volume fractions.

Equation VI shows the calculation of the shear modulus of a bulk by considering the crystalline volume fraction ω, the shear modulus of the amorphous phase G_a, respectively, of the crystalline phase G_c and the reinforcement factor, also referred to as aspect ratio or geometric factor ξ which depends on the geometry of the inclusion, based on the Halpin−Tsai equation.[47,48]

$$G_{\text{eff}} = \frac{G_a[G_c + \xi(\omega G_c + (1-\omega)G_a)]}{\omega G_a + (1-\omega)G_c + \xi G_a} \quad \text{(VI)}$$

The aspect ratio ξ in the Halpin−Tsai equation is defined as $\xi = 2\,l/d$, where l and d refer to the largest diameter in longitudinal and transverse directions, respectively.

As the effective modulus of the bulk is known through experimental data, the amorphous modulus can be determined inversely under the use of the volume fraction of crystallinity, the shear modulus of the crystalline phase, and the aspect ratio.

To determine the volume fraction of crystallinity, the degree of crystallinity $\alpha(T,T_{\text{melt}})$ needs to be converted with the density of the crystal (ρ_c = 1.003 g/cm^3)[51] and the density of the sample. The shear modulus of the crystalline phase can be found in the literature[52] under the assumption of temperature-independent mechanical properties of the crystalline phase.

The relationship between the aspect ratio and the temperature will be assumed to have a linear correlation. It will be assumed that the first crystal formed below the melting temperature has a spherical shape, represented by an aspect ratio of 2. The second grid point to determine the linear change in aspect ratio will be obtained under ambient conditions from the literature for polyethylene according to refs 53−55.

2.4. Bulk Modulus of the Amorphous Phase. The compression modulus may be derived via equation VII under the assumption that the amorphous phase of the polymer has isotropic behavior.

$$K_a = \frac{2G_a(1+\nu_a)}{3(1-2\nu_a)} \quad \text{(VII)}$$

The amorphous shear modulus G_a is determined as described above, and the Poisson ratio of the amorphous phase ν_a will be assumed as 0.49 according to refs 56 and 57.

To estimate the solubility of a gas in a semicrystalline polymer using the SL-EOS and taking eigen pressure into account, it is necessary to determine the characteristic parameters for both the pure substances involved in the SL-

https://doi.org/10.1021/acs.jced.3c00429
J. Chem. Eng. Data XXXX, XXX, XXX−XXX

EOS model and the interaction parameter for the binary mixture (gas-polymer). The characteristic parameters of SL-EOS can be determined by modeling the *P-v-T* data of pure substances. In many cases, these characteristic parameters can be found in the existing literature.[27,58] The binary interaction parameter is determined by using experimental solubility data of the gas−polymer system, where the polymer is in the fully molten state at different temperatures.

In order to predict the gas solubility in semicrystalline polymers the eigen pressure needs to be determined under the consideration of several material parameters of the pure polymer, which are summarized in equation VIII.

$$P^{am} = P^{overall} + \alpha(T, T_{melt})(P^{eig}_{initialformation} + P^{eig}_{elasticmismatch}) \quad \text{(VIII)}$$

With this modeling approach, no model parameters need to be determined based on solubility data, where the polymer is in the semicrystalline state. Furthermore, in addition to what is discussed in ref 13 this modeling approach takes into account temperature-dependent mechanical properties of the amorphous phase of the pure polymer.

3. RESULTS AND DISCUSSION

The next section is structured as followed: First, the mathematical correlation of the temperature-dependent degree of crystallinity will be presented, following the determination of the characteristic parameters of polyethylene for the SL-EOS by modeling the *P-v-T* data of polyethylene with SL-EOS. In the next step, the interaction parameter k_{ij} of the SL-EOS will be determined by modeling the binary mixture of ethylene in polyethylene melts. Afterward, the amorphous shear moduli of polyethylene via the Halpin−Tsai equation are determined, based on the framework presented in the methods part. Lastly, the solubility of ethylene in polyethylene grades at further temperatures will be fully predicted, and the eigen pressure distributions will be presented and discussed.

3.1. Temperature Dependent Degree of Crystallinity.

The temperature-dependent degree of crystallinity of various polyethylene grades was measured by Starck et al.[44] and McKenna,[45] and this study subsequently developed a mathematical correlation to describe the temperature-dependent degree of crystallinity, as illustrated in Figure 2.

The experimental data were modeled analytically with functions of the following form and are hence correlations and not physically modeled:

$$\alpha(T) = a \exp(bT) + c \exp(dT) \quad \text{(IX)}$$

The parameters of the mathematical correlation are presented in Table 1 for certain degrees of crystallinities.

By utilizing this mathematical model, it is possible to determine the degree of crystallinity at various temperatures, if either the melting temperature or the degree of crystallinity at room temperature is known. As the coefficient of determination R^2 indicates by values close to 1, the mathematical correlation does represent the temperature-dependent degree of crystallinity of a polyethylene sample very well. For polyethylenes that have a different yet intermediate degree of crystallinity at ambient conditions as the measured data by Starck et al.[44] and McKenna,[45] at first approximation linear interpolation will be used to estimate their degree of crystallinity based on those polymers with the closest values to the desired extent. In the following, the degree of crystallinity at room temperature will be used to model the temperature-dependent crystallinity just as the melting temperature of the polyethylene, which will be used to describe the geometry of the crystalline phase in the Halpin−Tsai equation.

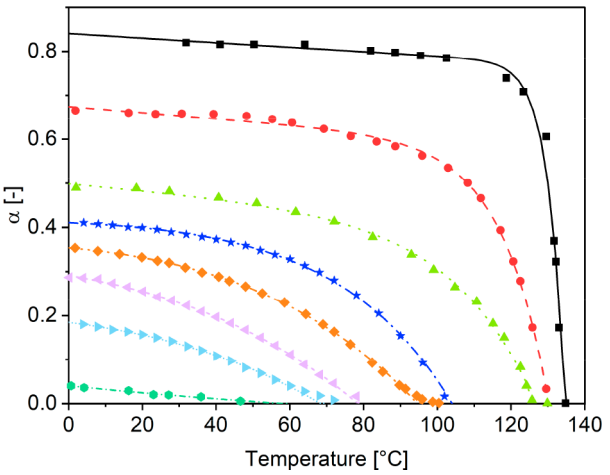

Figure 2. Temperature dependent degree of crystallinity of different polyethylene grades with a certain degree of crystallinity at room temperature against sample temperature. Experimental data from Starck et al.[44] and McKenna[45] with a certain degree of crystallinity at room temperature (points) and mathematical function (lines): 82% (black squares/solid line), 65% (red circles/dashed line), 49% (green triangles/dotted line), 39% (blue stars/dash dotted line), 32% (orange diamonds/dash dot dotted line), 24% (violet left triangles/short dashed line), 15% (light blue right triangles/short dotted line) and 2% (green hexagon/short dash dotted line). Uncertainty of measurements is not reported with data in the source.

3.2. Characteristic Parameters for SL-EOS.

Pure pressure−volume−temperature data for polyethylene melts were given by Zoller et al.[59] and Olabisi et al.[60] and will be used to determine the characteristic parameters of SL-EOS in this work for the polyethylene grades. For two linear high-density polyethylenes and two branched low-density polyethylenes, the specific volume is presented in the following figures at different pressures. The values account indirectly for the molecular structure of the polymers and are given in Table 2.

Table 2 presents data on the molecular architecture, in terms of molecular number and mass average, and the structure, in terms of density and degree of crystallinity, of the four different polyethylene grades investigated.[59,60] The molecular number and mass averages for these different grades vary between 18 to 28 kg mol^{-1} and 52 to 126 kg mol^{-1}, respectively. HDPE 1 has the highest molecular averages and a moderate degree of crystallinity at 62%, while HDPE 2 has the lowest molecular averages but the highest degree of crystallinity at 83%. The crystallinity range for LDPE grades falls between 42 to 50%. The pressure−volume−temperature data of these polyethylene grades at 0.1 MPa, 200 and 1000 bar can be seen in Figure 3 and are modeled by the SL-EOS with the characteristic parameters presented in this work (refer to Table 3).

The variation in specific volume among different grades of polyethylene is significant when they are in the semicrystalline state. This can be attributed to the different degrees of crystallinity, because of the difference in specific volume between fully amorphous and perfectly crystalline polyethylene. The experimental data of these polyethylene grades cover the whole spectrum from linear with high density to

https://doi.org/10.1021/acs.jced.3c00429
J. Chem. Eng. Data XXXX, XXX, XXX−XXX

Table 1. Parameters of the Mathematical Correlation (eq IX) of the Temperature-Dependent Degree of Crystallinity of Semicrystalline Polyethylene

α (20 °C)	a [-]	b [K^{-1}]	c [-]	d [K^{-1}]	R^2 [-]
82%	0.8408569	−0.0006335	0.0000000	0.2266211	0.9853
65%	−0.0000201	0.0789747	0.6742865	−0.0010358	0.9985
49%	−0.0014219	0.0447737	0.4998163	−0.0014802	0.9975
39%	−0.0165906	0.0315674	0.4269191	0.0003523	0.9989
32%	−0.1409568	0.0164774	0.4946908	0.0032106	0.9995
24%	−0.3851479	0.0119351	0.6761756	0.0047589	0.9995
15%	−0.9214604	0.0102140	1.1060609	0.0075400	0.9993
2%	−0.0198305	0.0067123	0.0602073	−0.0123969	0.9912

Table 2. Molecular Architecture of the Pure Polyethylene Grades for *P-v-T* Data[a]

		M_n [kg mol^{-1}]	M_w [kg mol^{-1}]	v (20 °C) [cm^3 g^{-1}]	α [%]	source
LDPE 1	branched	n.a.	n.a.	1.0881	42	59
LDPE 2	branched	25	100	1.0739	50	60
HDPE 1	linear	28	126	1.0537	62	59
HDPE 2	linear	18	52	1.0220	83	60

[a]Uncertainty of measurements is not reported with data in the source.

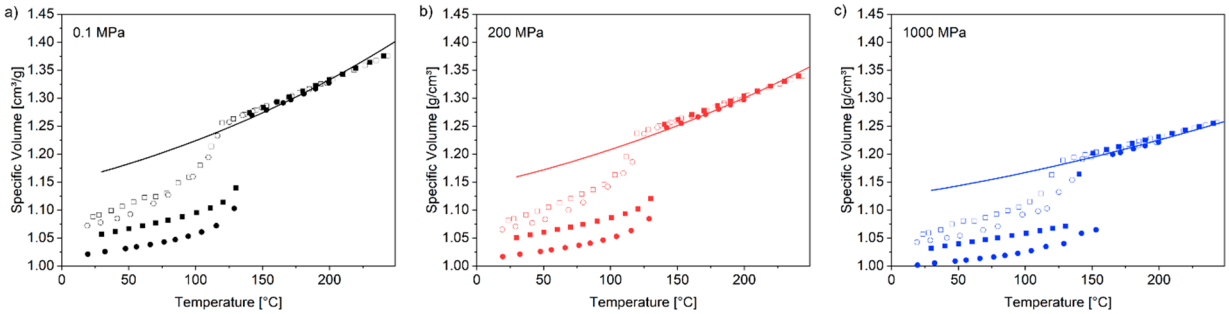

Figure 3. Specific volume of LDPE 1 (empty square), LDPE 2 (empty circles), HDPE 1 (full squares), HDPE 2 (full circle) against the temperature at (a) ambient pressure, (b) 200 MPa and (c) 1000 MPa measured by Zoller et al.[59] and Olabisi et al.[60] Modeled with SL-EOS in this work. Uncertainty of measurements is not reported with data in the source.

Table 3. Characteristic Parameters for the SL-EOS

	T^* [K]	P^* [MPa]	ρ^* [kg m^{-3}]	source
ethylene	283	339.5	680	56
polyethylene	633	473.3	913	this work

branched with low density. The polyethylene melt however does not indicate substantial differences in the *P-v-T* behavior with regard to the molecular architecture or branching. Hence, in this work, it will be assumed that for all grades, only one set of characteristic parameters will be used to describe the density of amorphous polyethylene melt neglecting any specific influence of its molecular architecture. The characteristic parameters of polyethylene can be found in Table 3. The characteristic parameters for ethylene were given by Alizadeh et al.[56] and are summarized in Table 3 as well.

3.3. Determination of the Binary Interaction Parameter k_{ij}. Various research groups[42,61−64] have conducted measurements to determine the solubility of ethylene in polyethylene. Maloney et al.[63] studied the solubility of ethylene in LDPE (low-density polyethylene) melt, which will be the basis for the interaction parameter identification in this work. By using these data and considering binary solubility data from other sources such as Chmelař et al.[42] and Novak et al.,[64] which investigated LLDPE (linear low-density polyethylene), MDPE (medium-density polyethylene), and HDPE (high-density polyethylene), respectively, the results are validated. Figure 4 presents both literature data and results obtained through modeling with SL-EOS in the fully molten state of the polymer.

The SL-EOS can describe the solubility of ethylene in molten polyethylene well. A linear correlation of the interaction parameter with the temperature could be observed, leading to eq X with a correlation coefficient R^2 = 0.9834.

$$k_{ij} = 0.000208T + 0.945280 \quad \text{(X)}$$

As shown in Figure 4, the solubility of ethylene does not change significantly with the molecular architecture and density of the polymer when it is in a molten state. This underpins why in this study it is assumed that the impact of molecular structure on ethylene solubility can be disregarded in the molten state. Consequently, only one correlation of the interaction parameter (eq X) will be used to forecast ethylene solubility in various grades of semicrystalline polymers.

3.4. Shear Modulus of the Amorphous Phase: Halpin−Tsai Model. To determine the amorphous shear modulus of polyethylene at different temperatures for different grades, experimental data from Illers[46] will be modeled with the Halpin−Tsai equation.[47,48] Kurita et al.[52] calculated the mechanical properties of various polymer crystals and proposed the value of 3406 MPa for the shear modulus of

https://doi.org/10.1021/acs.jced.3c00429
J. Chem. Eng. Data XXXX, XXX, XXX−XXX

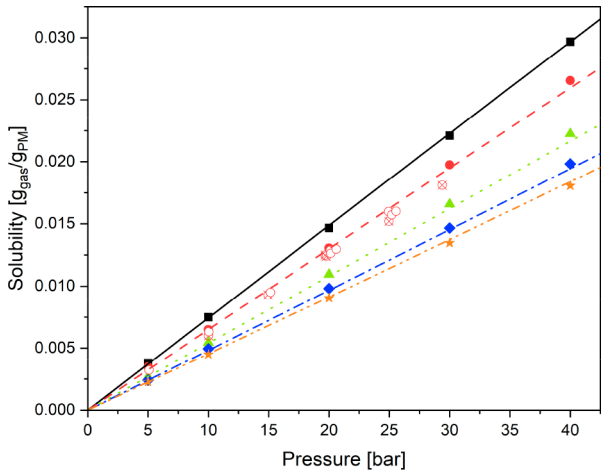

Figure 4. Solubility of ethylene in molten polyethylene against the pressure to determine interaction parameter k_{ij} as stated in eq X. Experimental data from Maloney et al.[63] at temperatures of 124 °C (black squares), 150 °C (red circles), 200 °C (green triangles), 250 °C (blue diamonds), and 300 °C (orange stars) with measurement uncertainty of 4%, 5%, 6%, 9%, and 10% at 124 °C, 150 °C, 200 °C, 250 °C, and 300 °C, respectively. Experimental data from Novak et al.[64] (red empty circles), relative measurement uncertainty of 1% and Chmelař et al.[42] (red crosses circles) at 150 °C, relative measurement uncertainty below 2%, respectively. Solid lines modeling with SL-EOS and k_{ij} in eq X in this work at 124 °C (black solid line), 150 °C (red dashed line), 200 °C (green dotted line), 250 °C (blue dash dotted line) and 300 °C (orange dash dot dotted line).

the crystalline phase. In this work, the shear modulus of the crystal will be assumed temperature-independent. In the Halpin−Tsai equation, the aspect ratio is defined as $\xi = 2\ l/d$. To account for changes in the geometry of the crystals in this work, the aspect ratio will be varied, assuming a linear correlation with the temperature. It will be assumed that after dropping below the crystallization temperature, initial crystals will take on spherical shapes, expressed by a geometric factor of 2. Each polyethylene grade's respective crystallization temperature will be calculated by utilizing the correlation of the temperature-dependent degree of crystallinity, presented in Figure 2. The second reference point used to determine the linear change in aspect ratio is set under ambient conditions. Gedde et al.[53] conducted Monte Carlo simulations to model the diffusion of *n*-hexane in polyethylene with degrees of crystallinity between 0 and 55%. Recently, Gedde et al.[53] proposed 5−25 as a realistic value range for the ratio of crystal diameter to length for polyethylene crystals. In the Halpin−Tsai equation this leads to geometric factors ξ from 10 to 50. In this work, no further overlay or orientation effects will be considered, so that the lowest aspect ratio will be applied for LLDPE and MDPE. The values from Gedde et al.[53] do not account for HDPE with a higher degrees of crystallinity, so the aspect ratio will be initially assessed on the basis of the orthorhombic lattice cell that Bunn[54] and Kim and Levon[55] stated for HDPE crystals with a diameter of 4.93 Å and a length of 7.39 Å, leading to an geometric factor ξ of 1.33.

Hereafter, the Halpin−Tsai equation (eq VI) can be solved inversely to determine the amorphous modulus of the different polyethylene grades with dependence on the geometric factor and their degree of crystallinity at room temperature. In this work, the described multiscale approach based on Fischlschweiger et al.[13] will be applied to various polyethylene−ethylene systems, whereby the polyethylene corresponds to different grades, varying from linear low-density polyethylene to high-density polyethylene from Chmelař et al.[42] The molecular architecture and morphology, especially the number-average molecular weight, the density, and the degree of crystallinity at ambient conditions of the polyethylene grades can be found in Table 4. There is no specific information on the branching of the polyethylene grades, but the architecture information in terms of branching is indirectly covered by morphological properties, i.e., degree of crystallinity.

Table 4. Molecular and Morphological Material Parameters of the Polyethylene Grades[a]

	M_n [kg mol^{-1}]	ρ [g cm^{-3}]	α(RT) [%]	source
LLDPE 1	35.4	0.915	45	42
LLDPE 2	34.3	0.923	51	42
MDPE 1	15.8	0.936	60	42
MDPE 2	17.3	0.938	61	42
HDPE 1	10.3	0.941	63	42
HDPE 2	N/A	0.950	69	42

[a]Uncertainty of measurements is not reported with data in the source.

By application of the Halpin−Tsai equation values for the amorphous shear modulus of these polyethylene grades are obtained and summarized in Table 5.

3.5. Prediction of the Solubility in the Semicrystalline State. This section will discuss the prediction of ethylene solubility in various semicrystalline grades of polyethylene. The prediction considers various factors, such as the molecular average weight number, the degree of crystallinity at ambient conditions, and the shear modulus of the amorphous phase at higher sample temperatures. All material parameters which are needed are determined in the sections above.

The prediction of the solubility of ethylene in two semicrystalline LLDPE grades is shown in Figure 5.

The SL-EOS under consideration of eigen pressure can predict the solubility of ethylene in LLDPE very well at temperatures from 60 to 100 °C. Especially in Figure 5b, where the solubility of the LLDPE 2 does show significant changes with the temperature, the model can describe the solubility very well. The shear modulus of the amorphous phase decreases with increasing temperature, resulting in a lower eigen pressure, which will be discussed later on in detail. Furthermore, solubility data from the amorphous melt at 150 °C of the LLDPE 2, which were already displayed in Figure 4, are presented in Figure 5b again for comparability. With only small deviations the SL-EOS predicts the solubility in the melt, thus verifying the usage of only one temperature-dependent interaction parameter for all grades.

In Figure 6 the solubility of ethylene in two semicrystalline MDPE grades is presented. The predicted solubility at lower temperatures, such as 60 and 80 °C, aligns well with data obtained from previous studies. At the highest measured temperature, 100 °C, slight deviations are noticeable (blue dash dotted line). This may be due to the reduced accuracy of the Halpin−Tsai equation at higher temperatures, resulting in an underprediction of the amorphous shear modulus and therefore an overprediction of the solubility.

Figure 7 presents the anticipated solubility isotherms for two different HDPE grades. The SL-EOS framework with the incorporation of eigen pressure leads to highly accurate and

https://doi.org/10.1021/acs.jced.3c00429
J. Chem. Eng. Data XXXX, XXX, XXX−XXX

Table 5. Amorphous Modulus of Different Polyethylene Grades against the Temperature of Solubility Isotherms[a]

	G(T) [MPa]					
	LLDPE 1	LLDPE 2	MDPE 1	MDPE 2	HDPE 1	HDPE 2
60 °C	26	19	20	22	-	-
80 °C	24	16	16	20	28	21
90 °C	21	-	-	-	19	-
100 °C	14	15	15	16	18	17
110 °C	-	-	-	-	16	-

[a]Uncertainty of calculations of ±6 MPa.

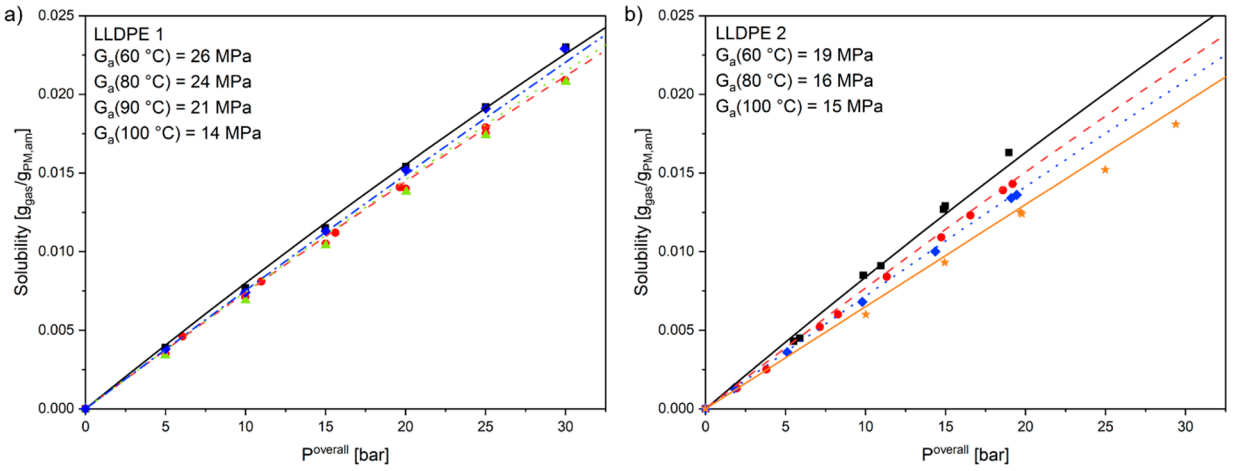

Figure 5. Solubility of ethylene against pressure in semicrystalline (a) LLDPE 1 (α(RT) = 45%, M_n = 35.4 kg mol^{-1}) at 60 °C (black squares), 80 °C (red circles), 90 °C (green triangles), and 100 °C (blue diamonds). (b) LLDPE 2 (α(RT) = 51%, M_n = 34.3 kg mol^{-1}) at 60 °C (black squares), 80 °C (red circles), and 100 °C (blue diamonds) and amorphous LLDPE 2 at 150 °C (orange stars). Experimental data from Chmelař et al.[42] and modeling this work with SL-EOS with P^{eig}. The relative standard uncertainty of the solubility $u_{(r)}(s_1)$ = 0.02.

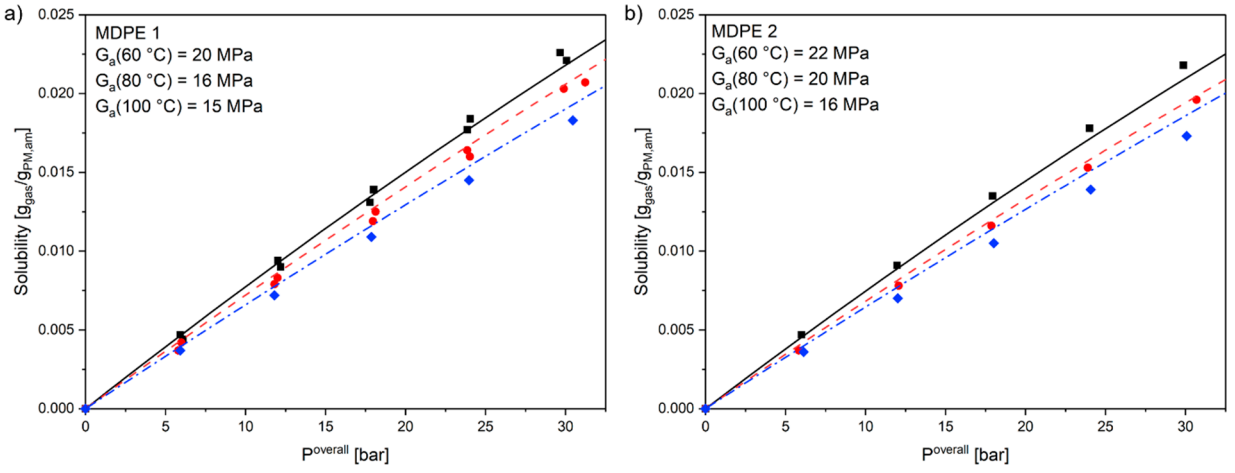

Figure 6. Solubility of ethylene against pressure in semicrystalline (a) MDPE 1 (α(RT) = 60%, M_n = 15.8 kg mol^{-1}) at 60 °C (black squares), 80 °C (red circles), and 100 °C (blue diamonds). (b) MDPE 2 (α(RT) = 61%, M_n = 17.3 kg mol^{-1}) at 60 °C (black squares), 80 °C (red circles), and 100 °C (blue diamonds). Experimental data from Chmelař et al.[42] and modeling this work with SL-EOS with P^{eig} at 60 °C (black solid line), 80 °C (red dashed line), and 100 °C (blue dash dotted line). The relative standard uncertainty of the solubility $u_{(r)}(s_1)$ = 0.02.

reliable prediction results. Similar to that for LLDPE 1, there are minimal variations in the solubility data for HDPE 1, making it challenging to assess the predictions accurately. In contrast, Figure 7b, shows slight changes in solubility with temperature for the second HDPE grade, which can be effectively represented by the model prediction. At a temperature of 100 °C, subtle divergences at higher pressures become apparent and can be attributed to the Halpin−Tsai equation, as discussed previously. The applicability of this model to other polymer gas systems however relies on having access to pure material parameters of the polymer in combination with solubility data in the polymer's molten state.

The evolution of the eigen pressure distribution for all investigated polymers can be seen in Figure 8. The data show how the eigen pressure, which represents the local mesophase stress within the different domains, changes concerning the overall pressure. It should be noted that the eigen pressure is ten times higher than the overall pressure. Furthermore, the

https://doi.org/10.1021/acs.jced.3c00429
J. Chem. Eng. Data XXXX, XXX, XXX−XXX

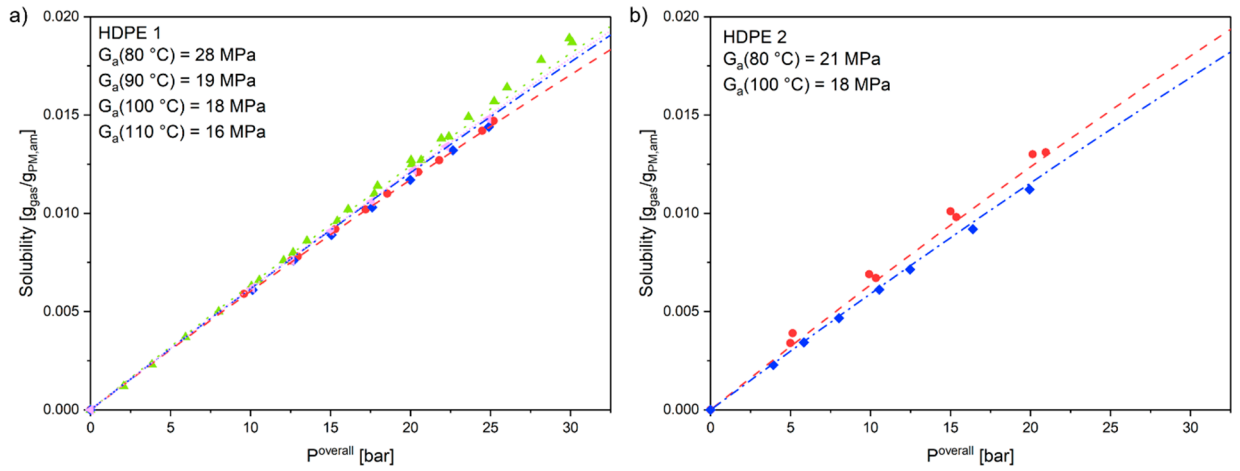

Figure 7. Solubility of ethylene against pressure in semicrystalline (a) HDPE 1 (α(RT) = 63%, M_n = 10.3 kg mol^{-1}) at 80 °C (red circles), 90 °C (green triangles), and 100 °C (blue diamonds) and 110 °C (violet left triangles). (b) HDPE 2 (α(RT) = 69%, M_n = N/A) at 80 °C (red circles) and 100 °C (blue diamonds). Experimental data from Chmelař et al.[42] and modeling this work with SL-EOS with P^{eig} at 80 °C (red dashed line), 90 °C (green dotted line), 100 °C (blue dash dotted line), and 110 °C (violet small dotted line). The relative standard uncertainty of the solubility $u_{(r)}(s_1)$ = 0.02.

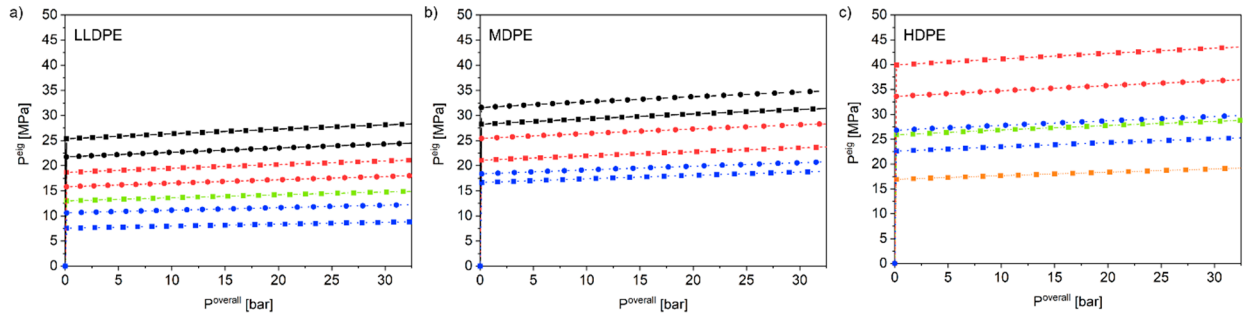

Figure 8. Eigen pressure distribution against the overall pressure in (a) LLDPE 1 (squares) and LLDPE 2 (circles), (b) MDPE 1 (squares) and MDPE 2 (circles), (c) HDPE 1 (squares) and HDPE 2 (circles) at 60 °C (black solid line), 80 °C (red dashed line), 90 °C (green dash dotted line), 100 °C (blue dotted line), 110 °C (orange short dotted line).

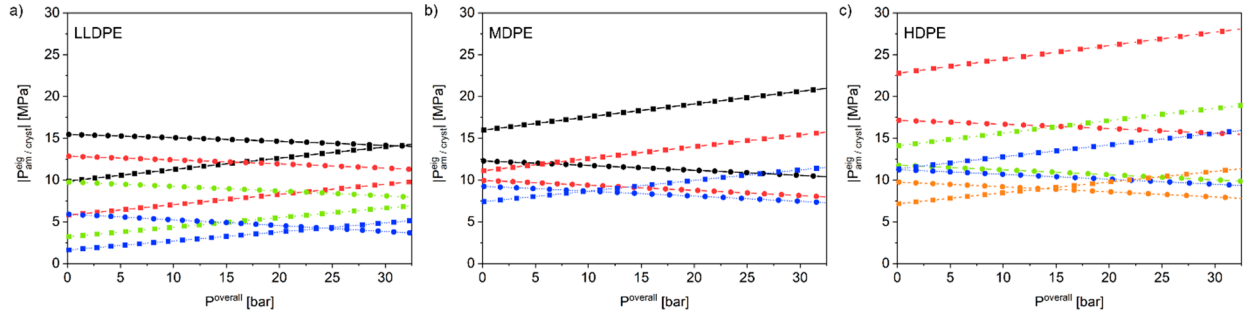

Figure 9. Comparison of amount of eigen pressure in the amorphous (squares) and crystalline (circles) phase against overall pressure in (a) LLDPE 1, (b) MDPE 1, and (c) HDPE 1 at temperatures of 60 °C (black solid line), 80 °C (red dashed line), 90 °C (green dotted line), 100 °C (blue short dotted line), and 110 °C (orange short dashed line).

eigen pressure follows a linear course over the overall pressure, resulting in higher eigen pressures when higher system pressures occur. This is based on the linear elastic material and spherical mechanical framework in this work. The eigen pressure decreases with increasing temperature, due to the decreasing amorphous shear modulus, the decreasing degree of crystallinity. This thermomechanic approach gives further access to the range of the internal eigen pressure of different polymer grades with varying degrees of crystallinity.

For the sake of comparison, we would like to mention, that Atiq et al.[65] fitted a constraint pressure in a semicrystalline HDPE-ethylene system based on solubility data in the semicrystalline polymer state and showed that the constraint pressure was around 32 MPa at 88 °C for the HDPE with a degree of crystallinity at room temperature between 67% to 70%. This corresponds closely to the predicted eigen pressure within this work of 30−34 MPa at 88 °C of the HDPE 2, which has a 70% degree of crystallinity, at the same overall pressure range from around 1 to 35 bar.

For a better understanding of the eigen pressure distribution, Figure 9 presents the eigen pressure in the amorphous and the

https://doi.org/10.1021/acs.jced.3c00429
J. Chem. Eng. Data XXXX, XXX, XXX−XXX

crystalline phase for LLDPE 1, MDPE 1, and HDPE 1 against the overall pressure, respectively.

As illustrated in Figure 8, the eigen pressure is predicted to decrease at higher temperatures due to the reduced degree of crystallinity and lower amorphous shear modulus. A similar trend can be observed in Figure 9 for the amount of pressure in the amorphous and crystalline phases. Furthermore, when considering degrees of crystallinity below 50%, such as that seen in LDPE 1, it is noted that at low overall pressures, the phase pressure within the crystalline phase exceeds that within the amorphous domains. This suggests that for low degrees of crystallinity, there is greater tension present within the crystals compared to the pressure experienced by the amorphous phase. In contrast, when the degree of crystallinity exceeds 50%, such as in HDPE 1, low system pressures result in higher pressure in the amorphous phase compared to the crystal domain. However, as overall pressure increases, there is a shift and the described effect reverses. This leads to higher tension in the crystal domain than compression in the amorphous phase. The reversal point is shifted further toward higher overall pressures with increasing temperature. For MDPE, shown in Figure 9b, the sorption temperatures range from 60 °C, over 80 to 100 °C, resulting in a degree of crystallinity decreased from 56.5% to 52.7% and then further down to 44.4%. At lower temperatures and therefore higher degrees of crystallinities, the pressure in the amorphous phase always exceeded that within the crystalline phase; however, this changed for an isotherm at 100 °C, where the pressure of the crystalline domain is around 2 MPa greater than in the amorphous phase.

4. CONCLUSIONS

The prediction of gas solubility in semicrystalline polymers plays an important role in many different applications, e.g., gas phase polymerization or the development of fuel cell membranes. To determine optimized process conditions, a prediction of the solubility at various pressures and temperatures below the melting temperature is necessary. Although the prediction for glassy polymers or polymer melts has been successfully shown, it is currently still a challenge to predict the solubility in the semicrystalline domains.

This contribution presents a new multiscale modeling approach to predict the solubility of gas in semicrystalline polymers at various temperatures and pressures for different polyethylene grades. The thermodynamic framework is based on the coupling of the SL-EOS with continuum mechanics developed by Fischlschweiger et al.[13] and complemented with a temperature-dependent degree of crystallinity as well as a mechanical homogenization method to account for changes in the crystalline geometry and local material properties in the amorphous and crystalline phases, respectively.

With this approach, a full prediction of the gas solubility in semicrystalline polymers becomes available, as the only parameter, which has to be determined based on experimental solubility data in the melt state, is the binary interaction parameter of the SL-EOS.

In this work, multiscale modeling is applied to predict the solubility of ethylene in various polyethylene grades. The solubility of ethylene could be predicted at temperatures from 60 to 110 °C and pressures from 1 to 30 bar. At very high degrees of crystallinity as well as high temperatures, the mechanical homogenization method with Halpin−Tsai equation results in slight deviations of the amorphous shear modulus and therefore of the solubility as well. In future work, different homogenization methods to account for the amorphous shear and compressive modulus should be tested to predict the solubility at high temperatures, and high degrees of crystallinities with even greater accuracy. In the future, numerical homogenization methods would be also of high interest to account for more complex crystal topologies on the mesoscale.

AUTHOR INFORMATION

Corresponding Author

Michael Fischlschweiger − *Chair of Technical Thermodynamics and Energy Efficient Material Treatment, Institute of Energy Process Engineering and Fuel Technology, Clausthal University of Technology, 38678 Clausthal, Zellerfeld, Germany;* orcid.org/0000-0002-0064-1292; Email: michael.fischlschweiger@tu-clausthal.de

Authors

Jana Zimmermann − *Chair of Technical Thermodynamics and Energy Efficient Material Treatment, Institute of Energy Process Engineering and Fuel Technology, Clausthal University of Technology, 38678 Clausthal, Zellerfeld, Germany*

Sabine Enders − *Institute of Technical Thermodynamics and Refrigeration Technology, Karlsruhe Institute of Technology (KIT), 76131 Karlsruhe, Germany;* orcid.org/0000-0002-4287-9936

Complete contact information is available at: https://pubs.acs.org/10.1021/acs.jced.3c00429

Author Contributions

Jana Zimmermann: methodology, software, formal analysis, data curation, writing-original draft, writing-review and editing, visualization, validation, conceptualization. Sabine Enders: conceptualization, writing-original draft, writing-review and editing. Michael Fischlschweiger: conceptualization, supervision, writing-original draft, writing-review and editing, project administration.

Notes

The authors declare no competing financial interest.

ABBREVIATIONS

HDPE, high-density polyethylene; LLDPE, linear low-density polyethylene; MDPE, medium-density polyethylene, PC-SAFT-EOS, Perturbed-Chain Statistical Associating Fluid Theory equation of state; PCP-SAFT-EOS, Perturbed-Chain Polar Statistical Associating Fluid Theory equation of state; SL-EOS, Sanchez−Lacombe equation of state

REFERENCES

(1) Nateghi, H.; Sodeifian, G.; Razmimanesh, F.; Mohebbi Najm Abad, J. A Machine Learning Approach for Thermodynamic Modeling of the Statically Measured Solubility of Nilotinib Hydrochloride Monohydrate (Anti-Cancer Drug) in Supercritical CO2. *Sci. Rep* **2023**, *13* (1), 12906.

(2) Hazazi, K.; Wang, Y.; Ghanem, B.; Hu, X.; Puspasari, T.; Chen, C.; Han, Y.; Pinnau, I. Precise Molecular Sieving of Ethylene from Ethane Using Triptycene-Derived Submicroporous Carbon Membranes. *Nat. Mater.* **2023**, *22*, 1218.

(3) Hassanpouryouzband, A.; Joonaki, E.; Taghikhani, V.; Bozorgmehry Boozarjomehry, R.; Chapoy, A.; Tohidi, B. New Two-Dimensional Particle-Scale Model To Simulate Asphaltene Deposi-

https://doi.org/10.1021/acs.jced.3c00429
J. Chem. Eng. Data XXXX, XXX, XXX−XXX

tion in Wellbores and Pipelines. *Energy Fuels* **2018**, *32* (3), 2661−2672.
(4) Pang, S.; Jin, S.; Yang, F.; Alberts, M.; Li, L.; Xi, D.; Gordon, R. G.; Wang, P.; Aziz, M. J.; Ji, Y. A Phenazine-Based High-Capacity and High-Stability Electrochemical CO2 Capture Cell with Coupled Electricity Storage. *Nat. Energy* **2023**, 1−11.
(5) Hassanpouryouzband, A.; Farahani, M. V.; Yang, J.; Tohidi, B.; Chuvilin, E.; Istomin, V.; Bukhanov, B. Solubility of Flue Gas or Carbon Dioxide-Nitrogen Gas Mixtures in Water and Aqueous Solutions of Salts: Experimental Measurement and Thermodynamic Modeling. *Ind. Eng. Chem. Res.* **2019**, *58* (8), 3377−3394.
(6) Moebus, J. A.; Greenhalgh, B. R. Modeling Vapor Solubility in Semicrystalline Polyethylene. *Macromol. React. Eng.* **2018**, *12* (4), 1700072.
(7) Sidhikku Kandath Valappil, R.; Ghasem, N.; Al-Marzouqi, M. Current and Future Trends in Polymer Membrane-Based Gas Separation Technology: A Comprehensive Review. *Journal of Industrial and Engineering Chemistry* **2021**, *98*, 103−129.
(8) Alassali, A.; Aboud, N.; Kuchta, K.; Jaeger, P.; Zeinolebadi, A. Assessment of Supercritical CO2 Extraction as a Method for Plastic Waste Decontamination. *Polymers* **2020**, *12* (6), 1347.
(9) Di Maio, E.; Kiran, E. Foaming of Polymers with Supercritical Fluids and Perspectives on the Current Knowledge Gaps and Challenges. *Journal of Supercritical Fluids* **2018**, *134*, 157−166.
(10) Zakaria, Z.; Kamarudin, S. K.; Wahid, K. A. A. Polymer Electrolyte Membrane Modification in Direct Ethanol Fuel Cells: An Update. *J. Appl. Polym. Sci.* **2023**, *140* (4), No. e53383.
(11) Sturm, D. R.; Caputo, K. J.; Liu, S.; Danner, R. P. Solubility of Solvents in Polyethylene below the Melt Temperature. *Fluid Phase Equilib.* **2018**, *470*, 68−74.
(12) Minelli, M.; De Angelis, M. G. An Equation of State (EoS) Based Model for the Fluid Solubility in Semicrystalline Polymers. *Fluid Phase Equilib.* **2014**, *367*, 173−181.
(13) Fischlschweiger, M.; Danzer, A.; Enders, S. Predicting Gas Solubility in Semi-Crystalline Polymer Solvent Systems by Consistent Coupling of Sanchez-Lacombe EOS with a Continuum Mechanics Approach. *Fluid Phase Equilib.* **2020**, *506*, 112379.
(14) Gross, J.; Sadowski, G. Perturbed-Chain SAFT: An Equation of State Based on a Perturbation Theory for Chain Molecules. *Ind. Eng. Chem. Res.* **2001**, *40* (4), 1244−1260.
(15) Gross, J.; Sadowski, G. Modeling Polymer Systems Using the Perturbed-Chain Statistical Associating Fluid Theory Equation of State. *Ind. Eng. Chem. Res.* **2002**, *41* (5), 1084−1093.
(16) Wiesmet, V.; Weidner, E.; Behme, S.; Sadowski, G.; Arlt, W. Measurement and Modelling of High-Pressure Phase Equilibria in the Systems Polyethyleneglycol (PEG)-Propane, PEG-Nitrogen and PEG-Carbon Dioxide. *Journal of Supercritical Fluids* **2000**, *17* (1), 1−12.
(17) Vogelpohl, C.; Brandenbusch, C.; Sadowski, G. High-Pressure Gas Solubility in Multicomponent Solvent Systems for Hydroformylation. Part I: Carbon Monoxide Solubility. *Journal of Supercritical Fluids* **2013**, *81*, 23−32.
(18) Vogelpohl, C.; Brandenbusch, C.; Sadowski, G. High-Pressure Gas Solubility in Multicomponent Solvent Systems for Hydroformylation. Part II: Syngas Solubility. *Journal of Supercritical Fluids* **2014**, *88*, 74−84.
(19) Tumakaka, F.; Gross, J.; Sadowski, G. Thermodynamic Modeling of Complex Systems Using PC-SAFT. *Fluid Phase Equilib.* **2005**, *228−229*, 89−98.
(20) van Schilt, M. A.; Wering, R. M.; van Meerendonk, W. J.; Kemmere, M. F.; Keurentjes, J. T.; Kleiner, M.; Sadowski, G.; de Loos, T. W. High-Pressure Phase Behavior of the System PCHC-CHO- CO2 for the Development of a Solvent-Free Alternative toward Polycarbonate Production. *Industrial & engineering chemistry research* **2005**, *44* (9), 3363−3366.
(21) Schäfer, E.; Vogelpohl, C.; Sadowski, G.; Enders, S. Simultane Modellierung von Phasengleichgewichten und Grenzflächeneigenschaften mithilfe des PCP-SAFT-Modells. *Chemie Ingenieur Technik* **2013**, *85* (10), 1512−1522.
(22) Gross, J.; Vrabec, J. An Equation-of-State Contribution for Polar Components: Dipolar Molecules. *AIChE J.* **2006**, *52* (3), 1194−1204.
(23) De Angelis, M. G.; Merkel, T. C.; Bondar, V. I.; Freeman, B. D.; Doghieri, F.; Sarti, G. C. Hydrocarbon and Fluorocarbon Solubility and Dilation in Poly(Dimethylsiloxane): Comparison of Experimental Data with Predictions of the Sanchez-Lacombe Equation of State. *J. Polym. Sci., Part B: Polym. Phys.* **1999**, *37* (21), 3011−3026.
(24) Enders, S.; Kahl, H.; Winkelmann, J. Interfacial Properties of Polystyrene in Contact with Carbon Dioxide. *Fluid Phase Equilib.* **2005**, *228−229*, 511−522.
(25) Rodgers, P. A.; Sanchez, I. C. Improvement to the Lattice-Fluid Prediction of Gas Solubilities in Polymer Liquids. *J. Polym. Sci., Part B: Polym. Phys.* **1993**, *31* (3), 273−277.
(26) Kiszka, M. B.; Meilchen, M. A.; McHugh, M. A. Modeling High-Pressure Gas-Polymer Mixtures Using the Sanchez-Lacombe Equation of State. *J. Appl. Polym. Sci.* **1988**, *36* (3), 583−597.
(27) Sanchez, I. C.; Lacombe, R. H. An Elementary Molecular Theory of Classical Fluids. Pure Fluids. *J. Phys. Chem.* **1976**, *80* (21), 2352−2362.
(28) Sanchez, I. C.; Lacombe, R. H. Statistical Thermodynamics of Polymer Solutions. *Macromolecules* **1978**, *11* (6), 1145−1156.
(29) Maity, S. K. Correlation of Solubility of Single Gases/Hydrocarbons in Polyethylene Using PC-SAFT. *Asia-Pac. J. Chem. Eng.* **2012**, *7* (3), 406−417.
(30) Bonavoglia, B.; Storti, G.; Morbidelli, M. Modeling of the Sorption and Swelling Behavior of Semicrystalline Polymers in Supercritical CO $_2$. *Ind. Eng. Chem. Res.* **2006**, *45* (3), 1183−1200.
(31) Valsecchi, M.; Ramadani, J.; Williams, D.; Galindo, A.; Jackson, G. Influence of Tie-Molecules and Microstructure on the Fluid Solubility in Semicrystalline Polymers. *J. Phys. Chem. B* **2022**, *126* (44), 9059−9088.
(32) Memari, P.; Lachet, V.; Rousseau, B. Molecular Simulations of the Solubility of Gases in Polyethylene below Its Melting Temperature. *Polymer* **2010**, *51* (21), 4978−4984.
(33) Memari, P.; Lachet, V.; Klopffer, M.-H.; Flaconnèche, B.; Rousseau, B. Gas Mixture Solubilities in Polyethylene below Its Melting Temperature: Experimental and Molecular Simulation Studies. *J. Membr. Sci.* **2012**, *390−391*, 194−200.
(34) Memari, P.; Lachet, V.; Rousseau, B. Gas Permeation in Semicrystalline Polyethylene as Studied by Molecular Simulation and Elastic Model. *Oil Gas Sci. Technol. - Rev. IFP Energies nouvelles* **2015**, *70* (2), 227−235.
(35) Michaels, A. B.; Haussleix, R. W. Elastic Factors Controlling Sorption and Transport Properties of Polyethylene. *J. polym. sci., C Polym. symp.* **1965**, *10* (1), 61−86.
(36) Nilsson, F.; Lan, X.; Gkourmpis, T.; Hedenqvist, M. S.; Gedde, U. W. Modelling Tie Chains and Trapped Entanglements in Polyethylene. *Polymer* **2012**, *53* (16), 3594−3601.
(37) Flory, P. J. Statistical Mechanics of Swelling of Network Structures. *J. Chem. Phys.* **1950**, *18* (1), 108−111.
(38) Panayiotou, C.; Sanchez, I. C. Swelling of Network Structures. *Polymer* **1992**, *33* (23), 5090−5093.
(39) Li, G.; Li, H.; Wang, J.; Park, C. B. Investigating the Solubility of CO2 in Polypropylene Using Various EOS Models. *Cellular Polymers* **2006**, *25* (4), 237−248.
(40) Markočič, E.; Škerget, M.; Knez, Ž. Effect of Temperature and Pressure on the Behavior of Poly(ε-Caprolactone) in the Presence of Supercritical Carbon Dioxide. *Ind. Eng. Chem. Res.* **2013**, *52* (44), 15594−15601.
(41) Becker, F.; Buback, M.; Latz, H.; Sadowski, G.; Tumakaka, F. Cloud-Point Curves of Ethylene-(Meth)Acrylate Copolymers in Fluid Ethene up to High Pressures and Temperatures—Experimental Study and PC-SAFT Modeling. *Fluid Phase Equilib.* **2004**, *215* (2), 263−282.
(42) Chmelař, J.; Smolná, K.; Haškovcová, K.; Podivinská, M.; Maršálek, J.; Kosek, J. Equilibrium Sorption of Ethylene in Polyethylene: Experimental Study and PC-SAFT Simulations. *Polymer* **2015**, *59*, 270−277.

https://doi.org/10.1021/acs.jced.3c00429
J. Chem. Eng. Data XXXX, XXX, XXX−XXX

(43) Feng, Z.; Panuganti, S. R.; Chapman, W. G. Predicting Solubility and Swelling Ratio of Blowing Agents in Rubbery Polymers Using PC-SAFT Equation of State. *Chem. Eng. Sci.* **2018**, *183*, 306−328.
(44) Starck, P.; Rajanen, K.; Lofgren, B. Comparative Studies of Ethylene-a-Olefin Copolymers by Thermal Fractionations and Temperature-Dependent Crystallinity Measurements. *Thermochim. Acta* **2002**, *395*, 169.
(45) McKenna, T. F. Solubility and Crystallinity Data for Ethylene/Polyethylene Systems. *Eur. Polym. J.* **1998**, *34* (9), 1255−1260.
(46) Illers, K.-H. Die Kristallinitätsabhängigkeit Der Dynamisch-Mechanischen Eigenschaften von Linearem Polyäthylen | SpringerLink. *Kolloid-Zeitschrift und Zeitschrift für Polymere* **1973**, *251* (251), 394−401.
(47) Affdl, J. C. H.; Kardos, J. L. The Halpin-Tsai Equations: A Review. *Polym. Eng. Sci.* **1976**, *16* (5), 344−352.
(48) Halpin, J. C.; Pagano, N. J. The Laminate Approximation for Randomly Oriented Fibrous Composites. *Journal of Composite Materials* **1969**, *3* (4), 720−724.
(49) Crist, B.; Fisher, C. J.; Howard, P. R. Mechanical Properties of Model Polyethylenes: Tensile Elastic Modulus and Yield Stress. *Macromolecules* **1989**, *22* (4), 1709−1718.
(50) Boyd, R. H. The Modulus of the Amorphous Component in Polyethylenes. *Polym. Eng. Sci.* **1979**, *19* (14), 1010−1016.
(51) Richardson, M. J.; Flory, P. J.; Jackson, J. B. Crystallization and Melting of Copolymers of Polymethylene. *Polymer* **1963**, *4*, 221−236.
(52) Kurita, T.; Fukuda, Y.; Takahashi, M.; Sasanuma, Y. Crystalline Moduli of Polymers, Evaluated from Density Functional Theory Calculations under Periodic Boundary Conditions. *ACS Omega* **2018**, *3* (5), 4824−4835.
(53) Gedde, U. W.; Unge, M.; Nilsson, F.; Hedenqvist, M. S. Mass and Charge Transport in Polyethylene - Structure, Morphology and Properties. *Polymer* **2023**, *266*, 125617.
(54) Bunn, C. W. The Crystal Structure of Long-Chain Normal Paraffin Hydrocarbons. The "Shape" of the < CH2 Group. *Trans. Faraday Soc.* **1939**, *35* (0), 482−491.
(55) Kim, M. S.; Levon, K. Crystallization and Phase Separation of High-Density Polyethylene in the Presence of Comb-like Polymer, Poly(Octadecyl Acrylate). *Eur. Polym. J.* **1997**, *33* (10−12), 1787−1798.
(56) Alizadeh, A.; Chmelař, J.; Sharif, F.; Ebrahimi, M.; Kosek, J.; McKenna, T. F. L. Modeling Condensed Mode Operation for Ethylene Polymerization: Part I. Thermodynamics of Sorption. *Ind. Eng. Chem. Res.* **2017**, *56* (5), 1168−1185.
(57) Sahputra, I. H.; Echtermeyer, A. T. Effects of Temperature and Strain Rate on the Deformation of Amorphous Polyethylene: A Comparison between Molecular Dynamics Simulations and Experimental Results. *Modelling Simul. Mater. Sci. Eng.* **2013**, *21* (6), 065016.
(58) von Konigslow, K.; Park, C. B.; Thompson, R. B. Evaluating Characteristic Parameters for Carbon Dioxide in the Sanchez-Lacombe Equation of State. *J. Chem. Eng. Data* **2017**, *62* (2), 585−595.
(59) Zoller, P.; Walsh, D. J. *Standard Pressure Vol. Temperature Data for Polymers*, 1st ed.; CRC Press, 1995.
(60) Olabisi, O.; Simha, R. Pressure-Volume-Temperature Studies of Amorphous and Crystallizable Polymers. I. Experimental. *Macromolecules* **1975**, *8* (2), 206−210.
(61) Rousseaux, P.; Richon, D.; Renon, H. Ethylene—Polyethylene Mixture: Saturated Liquid Densities and Bubble Pressures up to 26.1 MPa and 493.1 K. *J. Polym. Sci. Polym. Chem. Ed.* **1985**, *23* (6), 1771−1785.
(62) Heuer, T.; Peuschel, G.-P.; Rätzsch, M.; Wohlfarth, Ch. Untersuchungen zur Löslichkeit von Ethen, Propan, Propen und But-1-en in Schmelzen von Oligomeren des Polyethylens bzw. (Ethen-Vinylacetat)-Copolymeren bei Temperaturen bis 473,15 k und Drücken bis 30 MPA. Teil I. Apparaturen und Ergebnisse. *Acta Polym.* **1989**, *40* (4), 272−278.
(63) Maloney, D. P.; Prausnitz, J. M. Solubilities of Ethylene and Other Organic Solutes in Liquid, Low-Density Polyethylene in the Region 124° to 300°C. *AIChE J.* **1976**, *22* (1), 74−82.
(64) Novak, A.; Bobak, M.; Kosek, J.; Banaszak, B. J.; Lo, D.; Widya, T.; Harmon Ray, W.; de Pablo, J. J. Ethylene and 1-Hexene Sorption in LLDPE under Typical Gas-Phase Reactor Conditions: Experiments. *J. Appl. Polym. Sci.* **2006**, *100* (2), 1124−1136.
(65) Atiq, O.; Ricci, E.; Giacinti Baschetti, M.; De Angelis, M. G. Multi-Scale Modeling of Gas Solubility in Semi-Crystalline Polymers: Bridging Molecular Dynamics with Lattice Fluid Theory. *Fluid Phase Equilib.* **2023**, *570*, 113798.

https://doi.org/10.1021/acs.jced.3c00429
J. Chem. Eng. Data XXXX, XXX, XXX−XXX